Journal Name

ARTICLE

‘Overloading’ fluorescent silica nanoparticles with dyes to improve biosensor performance

Colin J. Moore,[a]† Giorgia Giovannini,[a] Filip Kunc,[a] Andrew J. Hall,[a] Vladimir Gubala[a]

Using dye-doped silica nanoparticles (DSNP) as reporter probes, we describe a simple method of enhancing fluorescent signal and the extension of the detectable target concentration range in a proof-of-concept ‘dissolution immunoassay’. DSNPs were *intentionally* ‘overloaded’ with 3% (w/w) FITC such that the high concentration of dye inside the NP core induced self-quenching. Despite exhibiting reduced brightness, the ‘overloaded’ DSNPs were then functionalized with anti-human IgG and were subsequently used to detect human IgG, a model biomarker, in whole serum. Following human IgG recognition, the ‘overloaded’ DSNPs were dissolved using pH10.6, 0.1M sodium carbonate-bicarbonate buffer. The large quantity of FITC inside the NP core was consequently released into solution, thus liberating the dyes from self-quenching, and led to a large increase in fluorecein emission intensity. This effect was further enhanced when coupled with FITC’s increased quantum yield in basic conditions. The overall result was a 12-fold enhancement in fluorescent signal intensity and an 11-fold improvement in signal-to-noise ratio after a dissolution time of 60 mins. In the assay setup presented, the net signal-to-noise ratio for ‘overloaded’ DSNPs was up to 9 times greater following degradation compared to traditionally used 1% (w/w) ‘optimal’ dye-loaded DSNPs. Crucially, this ‘dissolution assay’ strategy using ‘overloaded’ DSNPs could confidently detect human IgG at a 10-fold lower concentration than traditionally used ‘optimal’ DSNPs.

Introduction

Limit of detection, dynamic range, detection precision, and accuracy are some of the most important parameters describing the performance of any biomedical diagnostics device, particularly those used for early disease detection. [1-3]. Independent of the detection platform, a biosensors signal-to-noise ratio (S/N) governs both the sensitivity and the detectable concentration range [4, 5]. Ideally, the signal produced by the detection probe upon target recognition should be measurably high across a clinically relevant range of concentrations, whilst noise (i.e. non-specific binding) should be minimal in the absence of an analyte. Positive signal must be clearly discernible from noise to allow for confident target detection.

For fluorescence-based sensing, metal-enhanced fluorescence is a commonly employed approach to enhance the emission profile of probe fluorophores (typically an organic dye)[6, 7]. This approach therefore increases the positive-binding signal and, in turn, leads to an improvement in a sensors S/N ratio. Metal-enhanced fluorescence uses of metal colloids and nanoscale metallic nanostructures, such as thin films and islands, and offers the opportunity to modify fundamental properties of fluorophores in both near- and far-field fluorescence formats. However, despite the advancements in nanotechnology over the past two decades, such nano-structures/objects are still notoriously challenging to reliably prepare, handle and store with good colloidal stability[8]. They also often require expensive nanopatterning instrumentation, thus limiting their upscaling. Alternative, simple approaches to fluorescent signal enhancement are therefore needed.

Dye-doped silica NPs (DSNP) have become an attractive class of fluorescent probe due to their predictable chemistry and excellent optical properties, which have been reported to be comparable to quantum dots[9, 10]. The pioneering work of Tan, Wiesner and others made DSNPs very popular material used in imaging[11], sensing[12, 13] and drug delivery systems[14]. Achieving high brightness using silica NPs is possible by using large Stoke-shift organic dyes [15], and encapsulating new inorganic fluorophores such as QDs[16] or noble metal nanoclusters, as introduced by Le Guèvel[17]. However, considering cost of new mega-stokes organic dyes and some practical challenges related to the instability of the new generation of inorganic fluorophores, material scientists tend to use the well-characterized and inexpensive organic fluorophores such as fluorescein, rhodamine or some cyanine dyes (among others)[18]. These dyes typically have large absorbance/emission spectral overlap due to their sall Stokes shift.

This means high brightness in DSNP is achieved by optimizing the concentration of inexpensive dye molecules trapped inside the NP core: too few fluorophores result in an insufficiently bright NP, while a high concentration of

[a] *Medway School of Pharmacy, University of Kent, Chatham Maritime, Kent, ME4 4TB, United Kingdom. Corresponding author: V.Gubala@kent.ac.uk*

† CJM current address: FOCAS Research Institute, Dublin Institute of Technology, Kevin St, Dublin 8, Ireland

Electronic Supplementary Information (ESI) available: Detailed description of materials and methods (NP synthesis, bioconjugation, particle characterisation, dissolution studies). See DOI: 10.1039/x0xx00000x

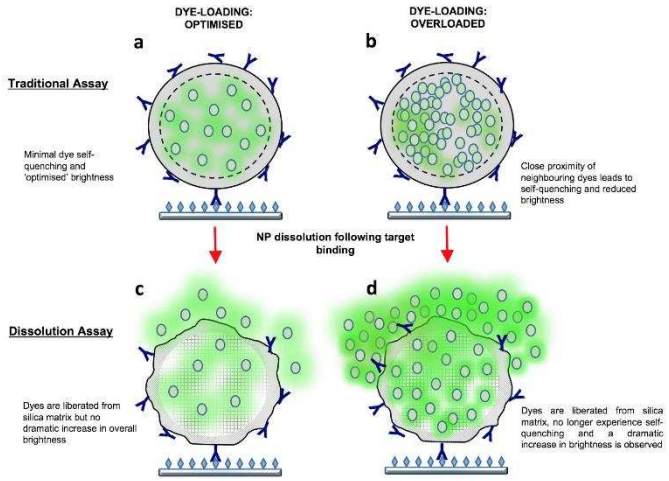

Figure 1: The traditional assay versus the dissolution assay. (a) Traditionally, fluorescent NP of 'optimal' dye-loading are used as fluorescent NP reporters. (b) NPs 'overloaded' with dyes lead to fluorophores in close proximity to each other and an overall reduction in NP brightness due to self-quenching. Following target binding we propose degrading the dye-loaded NPs using sodium carbonate-bicarbonate buffer (c) Dyes released from the 'optimally' loaded NPs are not expected to produce a large increase in fluorescent signal compared to before dissolution. (d) For 'overloaded' NPs, the dyes may be released from the silica matrix (via NP dissolution) such that they no longer experience self-quenching. Releasing a high concentration of dyes into solution would therefore lead to a large fluorescence increase. This simple method of achieving high fluorescence signal may prove superior to traditional NPs of 'optimised' loading.

fluorophores also results in reduced brightness. The later scenario is caused by self-quenching phenomena such as Förster resonance energy transfer (FRET), which occurs due to the dye's inherently small Stokes shift [19], and dye aggregation. Traditional DSNP synthesis approaches therefore attempt to maximize the number of organic dye molecules per NP before brightness begins to be compromised, i.e. 'optimized' DSNPs [20, 21]. Silica NPs 'overloaded' with fluorophores show reduced brightness, and they are typically considered to have no practical use and are usually discarded.

Here, a variation on the conventional approach of using 'optimised' DSNPs for biosensing is presented (**Figure 1**). The concept is based on using silica NPs *intentionally* 'overloaded' with FITC (which leads to reduced brightness). FITC was chosen as a good model dye because it is relatively inexpensive, popular fluorescent dye used in physical sciences and bio-sciences. Fluorescein is also known for its pH sensitivity and the self-quenching effect when encapsulated in the matrix of nanoparticles is well described in the literature[21-23]. A proof-of-concept immunoassay is performed in the traditional format with just one modification. In a classical setup, reporting nanoparticles with 'optimised' brightness (usually coated with antibodies or other recognition molecules) are allowed to react with the target analyte, non-specifically bound NPs are washed away from the detection surface and the signal is acquired (**Figure 1a**). In the new 'dissolution immunoassay', we employ 'overloaded' DSNPs (**Figure 1b**) and expose it to a basic buffered medium (sodium carbonate-bicarbonate) after the final washing step, which disintegrates the nanoparticles and allows the excess of the loaded FITC molecules to escape the NP core to freely fluoresce (**Figure 1d**). In addition, the high concentration of released fluorescein molecules can be intentionally exposed to a basic environment and fluoresce particularly intensely due to improved quantum yield[23]. In this case, an ultra-bright fluorescent signal resulting from the combination of two factors: i) dissolution of 'overloaded' DSNPs and ii) enhancement of FITC fluorescence at basic pH could be produced, which leads to improvements in S/N. The advances in microfluidics technologies also mean that the introduction and/or mixing of another reagent(s) in immunoassay formats is actually a relatively simple task, and means our 'dissolution immunoassay' approach could potentially be translated into miniaturized, fully-automated, point-of-care systems[24-26].

In this work, we have compared 'optimised' and 'overloaded' DSNPs in a model 'dissolution immunoassay' for the detection of human IgG in whole serum. The fluorescence intensities of both 'optimised' and 'overloaded' DSNPs with FITC were compared before and after dissolution at various pH (i.e. pH7, pH8.8 and pH10.6), and their respective resultant signal-to-noise ratios calculated. To support our findings, we have also performed full characterization of the prepared DSNPs, studied the self-quenching phenomenon, the disintegration of silica matrix and the profile of dye release from the DSNPs.

Results and Discussion

Preparation and characterisation of dye-doped silica NPs

Dye-doped silica NPs (DSNPs) exhibiting core-shell architecture were prepared using the reverse microemulsion system adapted from Bagwe *et al* [27]. The covalent binding between the FITC molecules and the silica matrix was facilitated by reacting FITC with (3-aminopropyl)trimethoxysilane (APTMS) to yield a FITC-APTMS molecule (ESI, **Figure S1**). This allowed the dye to be incorporated covalently into the NP core (concurrently with TEOS) via the hydrolysis and condensation of its methoxysilane moieties. Different amounts of FITC-APTMS, based on the % weight versus TEOS used in core formation (ESI, **Table S1**), were added to the microemulsion system to produce NP cores of different dye loadings. The NP cores were later coated with a shell of silica, which enhances the optical properties of the DSNP[9, 10]. The shell was then functionalised with negatively charged phosphonate groups and reactive primary amino groups. The ratio of phosphonate groups to amine is optimised to provide a colloidally stable negatively charged NP whilst providing sites for surface functionalisation[21, 28].

DLS and TEM were used to examine the physicochemical characteristics of the prepared DSNPs (ESI, **Table S2**). Based on the DLS analysis, all dye-loaded NPs appeared similar in hydrodynamic diameter, polydispersity and zeta potential. The

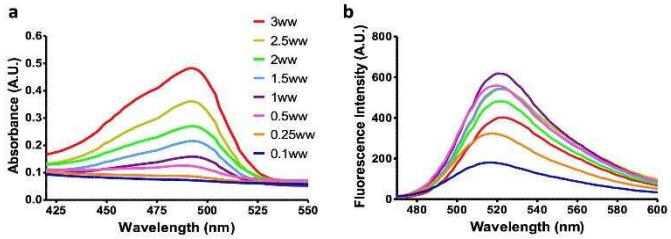

Figure 2: Absorbance and fluorescence emission spectra of silica NPs loaded with different concentrations of FITC. (a) According to absorbance measurements, more FITC was covalently bound into the silica NPs when more FITC-APTMS conjugate solution was introduced during particle synthesis. A maximum absorbance was seen at 492 nm for loadings of 0.5ww up to 3ww. (b) According to fluorescence emission scans, a loading of 1ww gave the brightest NP. More heavily doped NPs, such as 3ww, had reduced brightness presumably due to self-quenching mechanisms like FRET. Nanoparticles loaded with 1ww and 3ww FITC were subsequently called $NP_{OPTIMISED}$ and $NP_{OVERLOADED}$, respectively.

Z-average values for NP diameter ranged from 109-116 nm, and suggested that the addition of the FITC-APTMS conjugate did not play an influential role in the reverse microemulsion system employed here. The hydrolysis of the dye-conjugate produces methanol, which can influence micelle rigidity and micelle collision dynamics. However, when increasing amounts of dye-conjugate were used the amount of methanol generated did not appear to be influential in the resultant DSNP size or size distribution. The size and spherical shape was also corroborated by TEM (micrographs shown in **Figure S2**). TEM analysis showed that the diameter of DSNPs ranged between 46 and 53 nm. The zeta potential of all dye-loaded NPs showed negative values between -43 and -48 mV, thus suggesting high colloidal stability in aqueous conditions.

Once it was established that the NPs were colloidally stable, their optical absorbance and emission profiles were recorded. The absorbance spectra (**Figure 2a**) showed an expected increase in absorbance signal (λ_{max} = 492 nm) with increased dye-loadings, thus sensibly suggesting that when more FITC-APTMS conjugate was added to the microemulsion system more dyes were incorporated inside the resulting NP. The trend in fluorescence emission profiles was significantly different (**Figure 2b**). As anticipated, an increased dye-loading in 0.1, 0.25, 0.5 and 1ww NPs correlated positively with an increase in the fluorescence signal. The loading concentration of 1% (w/w) resulted in the brightest NP. Dye-loading concentrations above 1% (w/w) resulted in DSNPs with less intense fluorescence emission. This was attributed to self-quenching phenomena, which presumably occurred due to the increased numbers of dye molecules per unit volume inside the NP.

A noticeable red shift in the emission peak from 516 nm to 525 nm was seen with increased dye-loading (ESI, **Figure S3**), for the DSNPs. A similar effect was observed by Imhof *et al* [29] when the authors increased the concentration of fluorescein covalently bound inside silica NPs. This red shift in emission maximum was explained as a decrease in excited state energy due to interactions between neighbouring dye molecules.

We have also attempted to quantify the number of dyes encapsulated in the DSNPs. To achieve this, an equivalent mass of DSNPs were firstly fully disintegrated to release their dye content into solution such that self-quenching would be eliminated and dyes would be capable of fluorescing freely.

Secondly, the fluorescence intensity of such liberated dye molecules was recorded, which allowed us to extrapolate the dye concentration per mass of DSNP using a FITC calibration curve (**Table 1**). The data suggested an almost linear correlation between the amount of dyes used in the synthesis and the amount of dyes entrapped inside the silica matrix.

Table 1: The number of dyes per NP was quantified. In agreement with the absorbance spectra in Figure 2a, when more dye was incorporated during NP synthesis more was bound inside the resultant NP. A linear increase in the number of dyes per NP was observed with increased dye-loading, with 1ww and 3ww resulting in 356 ± 20 and 2143 ± 449 respectively.

NP name	Dye Loading (w/w)	Dyes per NP
0.1ww	0.1	59 ± 6
0.25ww	0.25	160 ± 19
0.5ww	0.5	196 ± 6
1ww	1	356 ± 20
1.5ww	1.5	696 ± 25
2ww	2	814 ± 31
2.5ww	2.5	1007 ± 134
3ww	3	2143 ± 449

Considering the fluorescence data (**Figure 2b**), 1% (w/w) DSNPs with 356 ± 20 FITC molecules per NP were the brightest nanoparticles. Interestingly, 3% (w/w) particles with 2143 ± 449 dyes per NP were 33% less bright than their 1% (w/w) counterparts. DSNPs prepared with 1% (w/w) FITC were therefore considered to have an 'optimal' balance between dye-loading concentration and NP brightness ($NP_{OPTIMUM}$), whereas 3% (w/w) DSNPs displayed reduced brightness because of dye 'overloading' ($NP_{OVERLOADED}$). We have also synthesized DSNPs by the other commonly used silica NP synthetic strategy, the Stöber method. The data showed that the correlation between dye overloading and the overall brightness is not exclusive to the silica nanoparticles prepared by the reverse microemulsion approach (ESI, **Figure S4)**.

It is noteworthy to mention that specific to biosensor applications, the 'overloaded' 3% (w/w) DSNP would traditionally be overlooked in favour of the 'optimum' 1% (w/w) DSNP. However, we hypothesised that if the large dye cargo of $NP_{OVERLOADED}$ can be released from the particle core, this could lead to significant improvements in fluorescent enhancement and easier signal transduction for the detection of specific binding events in the immunoassays. Importantly, this enhancement could be even more amplified by using an aqueous medium at basic pH, as we have demonstrated that the fluorescence signal of FITC can be increased in basic buffered solutions (ESI, **Figure S5**). Both the 1% (w/w) and 3% (w/w) DSNPs were compared in terms of their performance when used in immunoassay. To simplify further analysis of the data

presented in this article, 3% (w/w) NPs were labelled as **$NP_{OVERLOADED}$**, while 1% (w/w) NPs were labelled as **$NP_{OPTIMUM}$**.

Functionalising $NP_{OPTIMUM}$ and $NP_{OVERLOADED}$ with antibodies

In order for both the $NP_{OPTIMUM}$ and $NP_{OVERLOADED}$ to be used in an immunoassay, they were functionalised with antibodies. The conjugation of antibodies to NPs was facilitated through the use of primary amine groups that were introduced on the NP surface during the post-coating step (i.e. silica NPs were allowed to react with mixture of organosilanes such as aminopropyl trimethoxysilane and 3-(trihydroxysilyl)propyl methylphosphonate). These amine groups serve as reaction sites where crosslinking molecules for biomolecules attachment could be bound. It was important to investigate that the fraction of amine-coated surface on both $NP_{OPTIMUM}$ and $NP_{OVEROADED}$ was identical. The number of reactive $-NH_2$ on the surface of the respective DSNPs was probed by ninhydrin reaction (ESI, **Table S3**). The data suggested that the number of reactive amines per nm^2 on the $NP_{OPTIMUM}$ and $NP_{OVERLOADED}$ surfaces were comparable, and shows that the different dye-loadings did not influence the synthetic process in a way that leads to different surface functionalisation chemistry. Polyaldehyde dextran was then used as a crosslinking agent to graft goat anti-human IgG to the surfaces of both DSNPs. The benefits of using polyaldehyde dextran as a crosslinking has previously been reported in our group[30]. The reaction mechanism involves a formation of imine groups (also known as Schiff base) between the polyaldehyde dextran and amino groups on the NP surface and ε-amino groups of Lysine, an abundant amino acid on the protein surface. Using this established conjugation protocol, $NP_{OPTIMUM}$ and $NP_{OVERLOADED}$ were coated with similar concentrations of protein, 3.39 ± 0.36 and 3.17 ± 0.86μg per mg of DSNPs respectively (ESI, **Table S4**). The importance of reducing the imine bond into a stable secondary amine bond using sodium borohydride was also shown (ESI, **Figure S6),** and resulted in 2.4 times more protein per DSNP than when no reduction step was performed.

Nanoparticle Dissolution

Transmission Electron Microscopy (TEM)

The dissolution of silica NP matrix is well-described in the literature[31, 32]. For example, Park *et al.* reported the degradation of silica NPs into hollowed spheres due to etching under basic conditions (0.04M ammonia, pH10.0)[33]. A mechanism whereby small 'seed pores' in the NP core merge into single voids was proposed, thus resulting in large well-defined hollows. Similarly, O'Connell *et al.* also reported on the degradation of Cy5-loaded silica NPs under basic conditions (sodium carbonate containing 0.5% (w/w) SDS, pH10.0). In their study, the Cy5-doped silica NPs were produced by reverse microemulsion method and they were degraded to release Cy-5 dyes from the NP, thus allowing the number of dyes per NP to be quantified[34]. Mahon *et al.* highlighted that silica NPs can degrade under *in vitro* conditions, with visual hollowing of NPs seen by TEM[35]. The authors also commented that higher temperature (i.e. 37 °C) led to more rapid degradation than those examined at room temperature.

Therefore, in order to perform the 'dissolution assay' proposed in Figure 1, conditions for the dissolution of $NP_{OPTIMUM}$ and $NP_{OVERLOADED}$ were explored. Sodium carbonate-bicarbonate buffer was chosen as the dissolution medium because it is inexpensive and its widespread use in laboratories. Its relatively mild basic character means that it could also be easily incorporated into standard operating procedures of immunoassays or integrated into microfluidic devices. The basicity of sodium carbonate-bicarbonate buffer was stable across a broad pH range and therefore it was possible to examine the effect of pH on the rate of silica dissolution (pH 8.8 and 10.6). The time-scale of silica degradation is of importance for biosensors as achieving test results within a minimal timeframe is often required. DI water (pH 7.0) was also chosen as a dissolution medium such that the need for basic degradation conditions could be evaluated.

Initial experiments using plain $NP_{OPTIMUM}$ and $NP_{OVERLOADED}$ (i.e. NPs without dextran or antibody coatings) were performed by TEM as a method of detecting any NP hollowing. An observed hollowing would be attributed to NP degradation akin to the structures reported by Park[33], O'Connell[34] and Mahon[35]. $NP_{OPTIMUM}$ and $NP_{OVERLOADED}$ were incubated in the corresponding degradation medium (DI water, pH8.8 or pH10.6 buffer) for 0, 2 and 4 hours at 37 °C. The particles were then isolated via centrifugation, washed to remove salts and added to TEM grids to visualize changes in NP structure and morphology (**Figure 3**). For $NP_{OPTIMUM}$ all colloids appeared intact at 0 hours (i.e. upon immediately being dispersed in dissolution media). $NP_{OPTIMUM}$ also appeared intact in DI water even after 4 hours. However, clear hollowing was seen for the $NP_{OPTIMUM}$ in pH 8.8 and pH 10.6 buffers after only 2 hours. For NP samples incubated in pH 10.6 buffer, larger degree of degradation was observed when compared to those in pH8.8 environment. This was attributed to the accelerated hydrolysis of the silica matrix at more basic conditions. At pH 8.8, further hollowing had taken place between 2 and 4 hours for $NP_{OPTIMUM}$, as clearly visualized by TEM. It is important to note that the TEM images were taken of DSNPs that could be isolated into pellet form by centrifugation. As the DSNPs continued to degrade, especially in pH 8.8 and 10.6 buffers, the masses of $NP_{OPTIMUM}$ isolated continued to decrease, which was visible to a naked eye. Consequently, after 4 hours at pH 10.6, no $NP_{OPTIMUM}$ were isolated and it was only possible to visualise NP 'dissolution residue' by TEM, thus showing $NP_{OPTIMUM}$ had been virtually fully disintegrated after this time.

$NP_{OVERLOADED}$ dissolution followed similar trend as the $NP_{OPTIMUM.}$ $NP_{OVERLOADED}$ appeared intact upon initial dispersion in all studied media with no hollowing observed. After 2 hours in pH10.6 buffer, a miniscule NP pellet was obtained following

centrifugation and thus suggested large-scale dissolution of the nanomaterial. All $NP_{OVERLOADED}$ in pH8.8 buffer exhibited hollowing of their cores after 2 hours, which was not seen for 1% (w/w) $NP_{OPTIMUM}$. Additionally, $NP_{OVERLOADED}$ suspended in DI water displayed some hollowing after 2 hours. Similarly to $NP_{OPTIMUM}$, only 'dissolution residue' was observed for $NP_{OVERLOADED}$ after 4 hours in pH 10.6 solution, which was attributed to complete NP degradation. Larger hollows were seen at pH 8.8 after 4 hours compared to those after 2 hours, and suggested the remaining NPs capable of forming a NP pellet had undergone continued core dissolution. More hollow structures were seen after 4 hours for $NP_{OVERLOADED}$ in DI water compared to $NP_{OPTIMUM}$.

Overall, TEM analysis indicated that more rapid DSNP degradation occurred under the basic pH solutions, and was particularly pronounced in pH10.6 buffer.

Fluorescence Analysis

We have established that the silica matrix of the prepared DSNPs could be effectively degraded using simple, basic buffered solutions. In addition, we have also shown that fluorescence emission of FITC is enhanced in basic buffered solutions (ESI, **Figure S4**). In order to investigate the FITC leaching profile, we have used antibody-coated NPs (Ab-$NP_{OVERLOADED}$ and Ab-$NP_{OPTIMUM}$) and incubated them over time

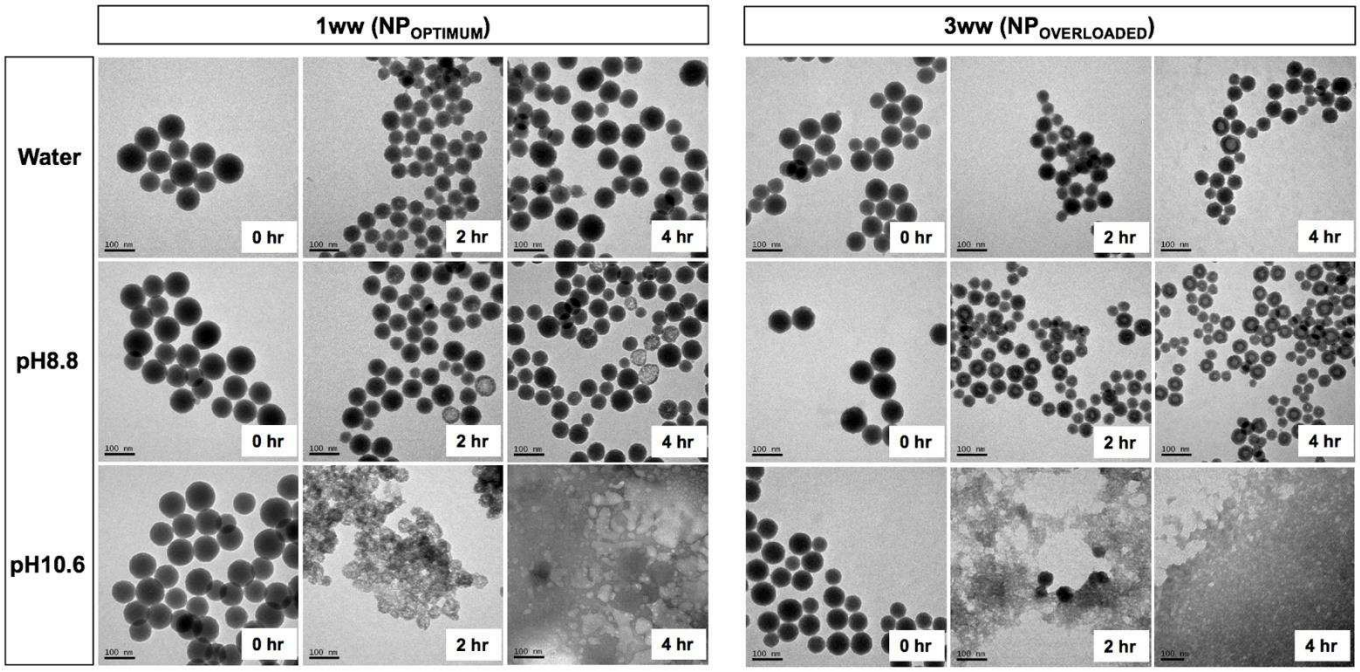

Figure 3: Dissolution of plain NPs over time in three different media at 37 °C: pH 7.0 DI water, pH 8.8 sodium carbonate-bicarbonate buffer and pH 10.6 sodium carbonate-bicarbonate buffer. The most rapid NP dissolution conditions for $NP_{OVERLOADED}$ was observed at pH 10.6. Overall, the dissolution rate appeared to be faster for $NP_{OVERLOADED}$ compared to $NP_{OPTIMISED}$. After 4 hours in pH 10.6 solution no NPs were observed and only particle 'debris' could be seen.

Interestingly, it was clear from the TEM micrographs that the rate of degradation for $NP_{OPTIMUM}$ and $NP_{OVERLOADED}$ was different. $NP_{OVERLOADED}$ appeared more harshly degraded and hollowed than their $NP_{OPTIMUM}$ counterparts. We propose that the silica matrix of the maximally loaded 3% (w/w) nanoparticles is less densely crosslinked than 1% (w/w) $NP_{OPTIMUM}$. When high loading of dye was used, NPs with less dense (i.e. more porous) silica network could have been created (ESI, **Figure S7**). Therefore, the hydrolysis and silica degradation of the less densely crosslinked matrix (i.e. $NP_{OVERLOADED}$) was faster when compared to the more highly crosslinked silica matrix (i.e. $NP_{OPTIMUM}$). The net result was that the $NP_{OVERLOADED}$ underwent more rapid degradation.

in pH 7.0 DI water, pH 8.8 and pH 10.6 solutions at a concentration of 10 µg/mL and 50 µg/mL (5% and 25% of the Ab-NPs concentration introduced in the 'dissolution assay', realistically representing the concentration of Ab-NPs available for the 'dissolution' after the final washing step). Ab-NP dye release was also measured at two different temperatures, room temperature and 37 °C, to verify the influence of temperature on the silica degradation.

A notable trend evident in **Figure 4** was the difference in time taken for the fluorescence to plateau at room temperature and 37°C. At room temperature, the equilibrium was slowly reached between 6-8 hours (**Figure 4a, b**). The dissolution of the nanoparticles and the subsequent dye release was relatively slow. At 37 °C however, an observable acceleration in the rate of dye leaching was observed for both concentrations (**Figure**

4c, d). This trend of accelerated silica degradation at 37 °C was consistent with previous reports [33, 35].

Crucially, the fluorescence emission intensity of Ab-$NP_{OVERLOADED}$ was significantly higher when compared to that of Ab-$NP_{OPTIMUM}$. This effect is best illustrated on Ab-$NP_{OVERLOADED}$ and Ab-$NP_{OPTIMUM}$ samples measure in 'Water'. The Ab-$NP_{OVERLOADED}$ (red line) significantly outperformed their Ab-$NP_{OPTIMUM}$ (black line) counterparts over time (most dramatically seen on **Figure 4b** and **4d**). The sharp increase in fluorescence intensity for Ab-$NP_{OVERLOADED}$ was accredited to the liberation of the large amount of FITC molecules, fluorescence of which was no longer inhibited by self-quenching. In this case (i.e. in water), the pH effect didn't play any significant role. However, further enhancement can be achieved when the DSNPs are degraded at basic conditions (ph8.8-orange and ph10.6-purple line). At higher pH, both the reaction kinetics of the degradation of the silica matrix and the FITC emission signal are enhanced, which contributes to the overall fluorescence intensity.

Dissolution Assay and Signal Amplification

Ab-$NP_{OPTIMUM}$ and Ab-$NP_{OVERLOADED}$ were compared in a direct binding assay performed in 96-well plate format. **Figure 5a** illustrates the simplified, direct-binding assay model. Solutions of human IgG (50 nM, 5 nM or 0.5 nM) were added to the wells and the protein was adsorbed to the bottom (**Figure5a(i)**). Bovine serum albumin (BSA) was then used as a blocking agent to minimize Ab-NP non-specific binding on the well surface (**Figure 5a(ii)**). Then, anti-human IgG coated Ab-$NP_{OPTIMISED}$ or Ab-$NP_{OVERLOADED}$ suspended in whole serum were added to the wells and allowed to react with the adsorbed human IgG target (**Figure 5a(iii)**). We reasoned that it was important to perform assays in whole serum as it provided more realistic conditions to test the binding capacity of Ab-NPs. It also allowed us to consider the effects of protein corona on the Ab-NP surface[36]. We have previously shown how performing a direct binding assay in increasingly complex media (PBS, 10% serum, whole serum) reduces target recognition by Ab-NPs[30].

Traditionally, step iii (**Figure 5a**) is followed by the removal of unbound Ab-NPs and the fluorescent signal is read and interpreted. However, our 'dissolution assay' format introduced a simple step that involved the addition of 'dissolution medium' (i.e. DI water, pH 8.8 buffer or pH 10.6 buffer) (**Figure 5a(iv)**). The benefits of such assay modification are twofold: 1) Ab-$NP_{OVERLOADED}$ would release their high FITC cargo into solution, thus liberating the dyes from the silica matrix to escape self-quenching, thus enabling them to fluoresce freely; 2) exposing fluorescein to a basic environment improves its quantum yield, which leads to an increase in fluorescence emission intensity. Both factors coupled together could lead to fluorescence signal enhancement and improvements in the immunoassay S/N.

In parallel, control experiments in the absence of human IgG were performed to estimate the non-specific signal (i.e. noise) generated by the Ab-NPs (ESI, **Figure S8**). We also calculated the signal-to-noise ratio (S/N) before and after Ab-NP degradation, which would allow the merits of the 'dissolution assay' approach (**Figure 5a(iv)**) to be compared to traditional DSNP sensing (**Figure 5a(iii)**).

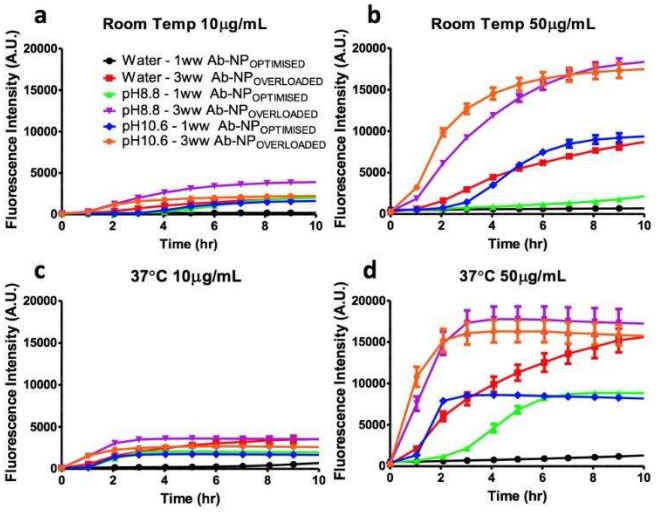

Figure 4: Fluorescent signal change of antibody-coated NPs (Ab-NP), 10 μg/mL or 50 μg/mL, undergoing dissolution at room temperature (RT) or 37°C . Fluorescein emission intensity was monitored over time as an indication of dye release from the Ab-NPs. (a) At RT, 10 μg/mL of Ab-NP take 6-8 hours before reaching a maximum and plateauing. (b) 50 μg/mL Ab-NP also took 6-8 hours to exhibit a maximum fluorescence during degradation at RT. (c) At 37 °C, the use of pH 8.8 and pH 10.6 sodium carbonate-bicarbonate buffer led to a large increase in emission intensity in FITC emission for 10 μg/mL Ab-NP after 2 hours and plateaued after 4 hours. (d) 50 μg/mL Ab-NPs degraded at 37 °C reached a maximum emission intensity and plateaued after 4 hours. Overall, degradation at 37 °C led to more rapid fluorescence intensity increases compared to RT, and was attributed to faster Ab-NP degradation at the elevated temperature. The pH sensitivity of FITC also meant increased dye quantum yield and more efficient emission in basic conditions.

The use of 0.1 M pH 10.6 sodium carbonate-bicarbonate buffer for NP dissolution afforded the best fluorescence signal enhancement (**Figure 5b, c, d**) when compared to pH 7.0 DI water and 0.1 M pH 8.8 sodium carbonate-bicarbonate. The data from the dissolution assay generated using DI water and pH 8.8 are shown in the ESI (**Figure S9** and **S10 respectively**). For clarity, the data shown in **Figure 5b, c, d** are also provided in **Table 2**.

Before the degradation had taken place (i.e. Traditional Assay, Table 2), Ab-$NP_{OPTIMUM}$ exhibited greater fluorescence intensity and S/N than Ab-$NP_{OVERLOADED}$ for all three concentrations of the human IgG target. This was because intact $NP_{OPTIMUM}$ were inherently brighter than $NP_{OVERLOADED}$, and would 'traditionally' justify the use of $NP_{OPTIMUM}$ for immunoassay applications. For example, at 0 minutes in **Figure 5b**, the S/N of Ab-$NP_{OPTIMUM}$ and Ab-$NP_{OVERLOADED}$ was 3.86 and 3.14 respectively. The background response (i.e. noise) generated by Ab-$NP_{OPTIMUM}$ and Ab-$NP_{OVERLOADED}$ (BSA wells) was negligibly low.

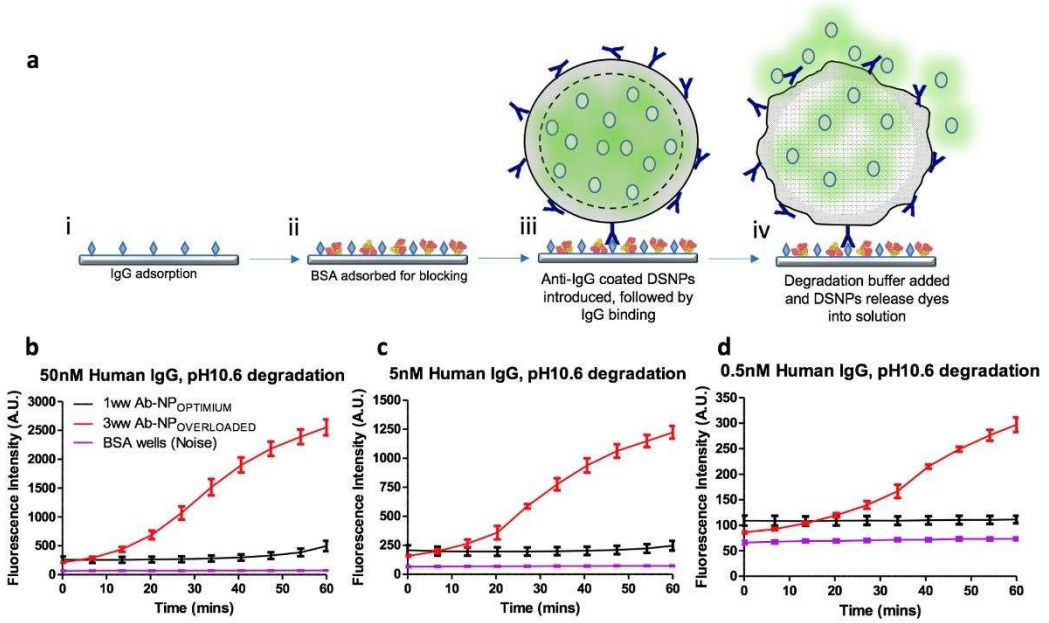

Figure 5: Dissolution direct binding assay for the detection of human IgG in whole serum. **(a,i)** Human IgG [50 nM, 5 nM or 0.5 nM] was incubated in a 96-well plate to absorb the protein to the well surface. **(ii)** BSA was then adsorbed to block the wells, thus minimizing the potential for non-specific binding. **(iii)** Anti-IgG-coated DDNPs (produced using either $NP_{OPTIMUM}$ or $NP_{OVERLOADED}$) were incubated in whole serum with the IgG-coated surface. The fluorescent signal produced by these intact antibody-coated DDNPs is the traditional way to use fluorescent silica NPs labels **(iv)** Adding 0.1 M pH 10.6 sodium carbonate-bicarbonate to the 96-well plate to degrade the Ab-NPs and released fluorescein from the DDNP core. **(b)** High concentrations of human IgG (50 nM) could be well discerned from background signal. After 60mins degradation, the fluorescence intensity of fluorescein in Ab-$NP_{OVERLOADED}$ was enhanced 12.1-fold and was superior to the signal produced by Ab-$NP_{OPTIMUM}$ **(c)** A similar trend was seen when detecting 5 nM human IgG **(d)** Degrading Ab-$NP_{OVERLOADED}$ allowed 0.5 nM human IgG to be confidently detected above background. This was not the case for Ab-$NP_{OPTIMUM}$. Using Ab-$NP_{OVERLOADED}$ therefore extended the working range of the assay by an order of magnitude. See **Table 2** for fluorescent values and S/N calculations.

While Ab-$NP_{OPTIMISED}$ were initially brighter than Ab-$NP_{OVERLOADED}$, the introduction of pH 10.6 buffer for particle dissolution led to a rapid increase in fluorescence for Ab-$NP_{OVERLOADED}$. Based on the data shown in **Figure 5b, c, d,** the fluorescence signal intensities from Ab-$NP_{OVERLOADED}$ wells had surpassed that of Ab-$NP_{OPTIMUM}$ already after 20 minutes, and steadily increased over the 60-minute period. Therefore, for the dissolution immunoassay, a maximum waiting time of 60 minutes was chosen for Ab-NP degradation.

The fluorescence signal intensity from wells with Ab-$NP_{OVERLOADED}$ after 60 minutes was enhanced 12.09-fold compared to the same system before dissolution (**Figure 5b)**. The S/N ratio reached 34.88; an 11.11 S/N enhancement. Overall, the fluorescence intensities of Ab-$NP_{OVERLOADED}$ and Ab-$NP_{OPTIMUM}$ after 60 minutes degradation time were 2553.50 and 497.00 respectively, and verified the hypothesis that 'overloading' DSNPs with fluorescein could lead into significant enhancement of fluorescence signal in immunoassay.

A similar trend was continued when 5 nM human IgG was adsorbed in the wells (**Figure 5c**). At 0 mins (Traditional Assay), Ab-$NP_{OPTIMUM}$ were superior fluorescent labels than Ab-$NP_{OVERLOADED}$. Ab-$NP_{OPTIMUM}$ exhibited a fluorescence intensity of 208.17 and S/N ratio of 3.14, while Ab-$NP_{OVERLOADED}$ exhibited a fluorescence intensity of 158.50 and S/N of 2.39. However, after dissolution the emission intensity from Ab-$NP_{OVERLOADED}$ wells was enhanced 7.72-fold and resulted in a S/N ratio of 16.67. This was considerably higher than the 1.19 and 3.37 fluorescence intensity and S/N enhancement afforded by Ab-$NP_{OPTIMUM}$ dissolution.

The most striking evidence of the benefits afforded by this dissolution assay strategy using Ab-$NP_{OVERLOADED}$ is shown in **Figure 5d** when detecting 0.5 nM IgG. At this concentration the S/N ratio of Ab-$NP_{OPTIMUM}$ was only 1.65 and was clearly approaching the limit of detection, leading to difficulties to discern positive target recognition from noise. This was even more evident for Ab-$NP_{OVERLOADED}$ at 0 minutes where a S/N ratio of 1.30 was produced. While the error bars for each data point in **Figure 5d** are narrow and do not overlap with those of the BSA coated wells (i.e. noise), it can be argued that there is insufficient confidence in the results to suggest positive target binding. However, after 60 minutes of NPs dissolution, it was clear that the fluorescent signal from Ab-$NP_{OVERLOADED}$ can be confidently detected above background signal. The fluorescence intensity after 60 minute for Ab-$NP_{OVERLOADED}$ was 297.00, a 3.45-fold enhancement compared to 0 minutes, and gave a S/N ratio of 4.05. On the other hand, no improvement in fluorescence signal was seen for Ab-$NP_{OPTIMUM}$ after 60min dissolution. Therefore, the use of Ab-$NP_{OVERLOADED}$ in a 'dissolution assay' format extended the dynamic range of the assay by an order of magnitude. It is also worthwhile noting that

the real concentration of human IgG absorbed to the sensor surface is presumably much lower than 0.5 nM as clearly not all of the target can be adsorbed to the well surface during the assay setup (**Figure 5a(i)**). Overall, the use of Ab-$NP_{OVERLOADED}$ in 'dissolution assays' has shown to be superior to the 'traditional' Ab-$NP_{OPTIMUM}$ approach. This is evident by the significant improvement in S/N exhibited by Ab-$NP_{OVERLOADED}$ after dissolution compared to the Ab-$NP_{OPTIMUM}$ when detecting the 50nM, 5nM and 0.5nM of human IgG respectively.

Considering the ease at which this dissolution step can be performed, this approach to performing immunoassays with silica NPs 'overloaded' with FITC may offer advantages to other fluorescence enhancement strategies that seek to improve signal-to-noise ratios. The reagents used in this work such as sodium carbonate-bicarbonate and FITC are also inexpensive, thus suggesting potential for this Ab-$NP_{OVERLOADED}$-based 'dissolution assay' to be widely adopted by research facilities and hospitals performing similar immunoassays. In addition, advances in microfluidic technology have demonstrated the possibility of housing and mixing liquids in a controllable fashion, which offers the potential for degradation buffers to be

Table 2: Fluorescence data from the 'dissolution assay' using pH10.6 sodium carbonate-bicarbonate are presented in Figure 5. Before dissolution (i.e. Traditional Assay), the fluorescent signal of Ab-$NP_{OPTIMUM}$ was superior to the signal produced by Ab-$NP_{OVEROADED}$ and resulted in the 'optimised' DSNPs exhibiting a better signal-to-noise (S/N) ratio. After 60min dissolution (i.e. Dissolution Assay) the fluorescent signal produced by Ab-$NP_{OVERLOADED}$ was superior to Ab-$NP_{OPTIMUM}$ when detecting the three different concentrations of human IgG. Dissolution resulted in improvements in Ab-$NP_{OPTIMUM}$ and Ab-$NP_{OVERLOADED}$ S/N, but was more pronounced for Ab-$NP_{OVERLOADED}$. Importantly, confidently detecting 0.5nM human IgG was possible for Ab-$NP_{OVERLOADED}$ but not Ab-$NP_{OPTIMUM}$ after dissolution (S/N of 4.05 and 1.52 respectively). The use of Ab-$NP_{OVERLOADED}$ in a 'dissolution assay' format can therefore extend the dynamic range of the assay by an order of magnitude. Overall, the S/N of Ab-$NP_{OVERLOADED}$ used in a 'Dissolution Assay' was 9.04, 5.31 and 2.45 times better than Ab-$NP_{OPTIMUM}$ used in a 'Traditional Assay' when detecting 50nM, 5nM and 0.5nM human IgG.

	Human IgG concentration	**50nM**			**5nM**			**0.5nM**	
		Ab-NP_{OPTMUM}	**Ab-$NP_{OVERLOADED}$**		**Ab-NP_{OPTMUM}**	**Ab-$NP_{OVERLOADED}$**		**Ab-NP_{OPTMUM}**	**Ab-$NP_{OVERLOADED}$**
Brightness	Traditional Assay	259.50	211.13		208.17	158.50		109.00	86.00
	Dissolution Assay	497.00	2553.50		247.00	1223.67		111.25	297.00
	Signal Enhancement Factor	1.92	12.09		1.19	7.72		1.02	3.45
S/N	Traditional Assay	3.86	3.14		3.14	2.39		1.65	1.30
	Dissolution Assay	6.79	34.88		3.37	16.67		1.52	4.05
	S/N Enhancement Factor	1.76	11.11		1.07	6.97		0.92	3.11
	$Traditional_{OPTIMUM}$ v $Dissolution_{OVERLOADED}$	1 : 9.04			1 : 5.31			1 : 2.45	

incorporated into lab-on-a-chip platforms. For example, Gomez-Blanco *et al* described a microfluidic device capable of pumping different reagents into their chip's sensing chamber[37]. The reagents were retained in an internal reservoir *via* a stop valve. This dissolution assay is 'proof-of-concept', therefore we also note that the 'overloaded' concentration of 3ww FITC-APTMS used during synthesis needs to be explored further in order to establish the dye loading concentration that generates the largest fluorescence signal and S/N enhancement possible. Nonetheless, the use of Ab-$NP_{OVERLOADED}$ in a 'dissolution assay' appears to be a simple, affordable and straightforward approach to enhancing immunoassay performance compared to traditional approaches.

Conclusions

A novel approach for the use dye-doped silica NPs (DSNPs) as fluorescent labels in immunoassays was presented. FITC was loaded into silica NPs and it was shown that a 1% (w/w) loading produced DSNPs with 'optimum' brightness, while 3% (w/w) overloading' produced DSNPs of reduced brightness. This reduction in brightness was attributed to the close proximity of neighbouring dyes inside the particle core that caused self-quenching due to phenomena such as homo-FRET and dye aggregation. Unlike traditional approaches to using DSNPs as fluorescent labels, we showed that the 'overloaded' DSNPs ($NP_{OVERLOADED}$) can exhibit more intense fluorescence emission than their 'optimally' loaded counterparts ($NP_{OPTIMUM}$). This was achieved by degrading the $NP_{OVERLOADED}$ under basic conditions such that their FITC content was released into solution, thus liberating the fluorophores from self-quenching and allowing them to fluoresce maximally. The basic conditions also improved the quantum yield of fluorescein, which further benefited fluorescent signal enhancement. $NP_{OPTIMUM}$ and $NP_{OVERLOADED}$ were functionalized with antibodies (Ab-$NP_{OPTIMUM}$ and Ab-$NP_{OVERLOADED}$ respectively) and used in a 'dissolution assay' performed in whole serum for the detection of human IgG. In all cases, the resultant fluorescent signal and signal-to-noise ratio following Ab-$NP_{OVERLOADED}$ dissolution was superior to those of Ab-$NP_{OPTIMUM}$ before dissolution. This confirmed the hypothesis that our 'dissolution assay' using silica NPs overloaded with fluorescein could outperform 'traditional assays' using in-tact optimally loaded NPs. This was attributed to the release of the high concentration of fluorescein from the

Ab-$NP_{OVERLOADED}$ and, in some cases, a 12-fold enhancement in fluorescent emission intensity. This in turn led to Ab-$NP_{OVERLOADED}$ exhibiting superior signal-to-noise ratios than Ab-$NP_{OPTIMIUM}$. Importantly, the 'dissolution assay' using Ab-$NP_{OVERLOADED}$ was capable of confidently detecting human IgG at an order of magnitude lower concentration than Ab-$NP_{OPTIMUM}$. Considering the fluorescent signal enhancements and signal-to-noise ratio improvements afforded by overloaded DSNPs, we believe that this simple method will be of interest for scientists developing immunoassays using dye-doped silica nanoparticles as fluorescent labels. In addition, this novel method is cost-effective and robust, and therefore offers an alternative approach to other fluorescent signal enhancement strategies like metal enhanced fluorescence.

Acknowledgements

CJM, GG and FK thank the University of Kent for the provision of their PhD scholarships.

1. V. Gubala, L. F. Harris, A. J. Ricco, M. X. Tan and D. E. Williams, *Anal. Chem.*, 2012, **84**, 487-515.
2. S. R. Teixeira, C. Lloyd, S. Yao, A. S. Gazze, I. S. Whitaker, L. Francis, R. S. Conlan and E. Azzopardi, *Biosens. Bioelectron.*, 2016, **85**, 395-402.
3. A. St John and C. P. Price, *Clin. Biochem. Rev.*, 2014, **35**, 155-167.
4. I. Heller, J. Männik, S. G. Lemay and C. Dekker, *Nano Lett.*, 2009, **9**, 377-382.
5. R. Peterson, B. Cunningham and J. Andrade, *FASEB J.*, 2014, **29**, 1
6. M. Bauch, K. Toma, M. Toma, Q. Zhang and J. Dostalek, *Plasmonics*, 2014, **9**, 781-799.
7. N. Sui, L. Wang, T. Yan, F. Liu, J. Sui, Y. Jiang, J. Wan, M. Liu and W. W. Yu, *Sens. Actuators B*, 2014, **202**, 1148-1153.
8. G. Giovannini, F. Kunc, C. C. Piras, O. Stranik, A. A. Edwards, A. J. Hall and V. Gubala, *RSC Advances*, 2017, **7**, 19924-19933.
9. H. Ow, D. R. Larson, M. Srivastava, B. A. Baird, W. W. Webb and U. Wiesner, *Nano Lett.*, 2005, **5**, 113-117.
10. A. Burns, H. Ow and U. Wiesner, *Chem. Soc. Rev.*, 2006, **35**, 1028-1042.
11. M. Benezra, O. Penate-Medina, P. B. Zanzonico, D. Schaer, H. Ow, A. Burns, E. DeStanchina, V. Longo, E. Herz, S. Iyer, J. Wolchok, S. M. Larson, U. Wiesner and M. S. Bradbury, *J. Clin. Invest.*, **121**, 2768-2780.
12. S. W. Bae, W. Tan and J.-I. Hong, *Chem. Commun.*, 2012, **48**, 2270-2282.
13. A. Burns, P. Sengupta, T. Zedayko, B. Baird and U. Wiesner, *Small*, 2006, **2**, 723-726.
14. A. Tivnan, W. S. Orr, V. Gubala, R. Nooney, D. E. Williams, C. McDonagh, S. Prenter, H. Harvey, R. Domingo-Fernandez, I. M. Bray, O. Piskareva, C. Y. Ng, H. N. Lode, A. M. Davidoff and R. L. Stallings, *PloS One*, 2012, **7**, e38129.
15. W. Pham, L. Cassell, A. Gillman, D. Koktysh and J. C. Gore, *Chem. Commun.*, 2008, **16**, 1895-1897.
16. S. Veeranarayanan, A. C. Poulose, M. S. Mohamed, Y. Nagaoka, S. Iwai, Y. Nakagame, S. Kashiwada, Y. Yoshida, T. Maekawa and D. S. Kumar, *Int. J. Nanomed.*, 2012, **7**, 3769-3786.
17. X. Le Guével, B. Hötzer, G. Jung and M. Schneider, *J. Mater. Chem.*, 2011, **21**, 2974.
18. A. Auger, J. Samuel, O. Poncelet and O. Raccurt, *Nanoscale Res. Lett.*, 2011, **6**, 328-328.
19. D. Genovese, S. Bonacchi, R. Juris, M. Montalti, L. Prodi, E. Rampazzo and N. Zaccheroni, *Angew. Chem. Int. Ed. Engl.*, 2013, **52**, 5965-5968.
20. G. Battistelli, A. Cantelli, G. Guidetti, J. Manzi and M. Montalti, *Wiley Int. Rev. Nanomed. Nanobiotechnol.*, 2016, **8**, 139-150.
21. R. I. Nooney, E. McCormack and C. McDonagh, *Anal. Bioanal. Chem.*, 2012, **404**, 2807-2818.
22. J. Fu, C. Ding, A. Zhu and Y. Tian, *Analyst*, 2016, **141**, 4766-4771.
23. R. Sjoback, J. Nygren and M. Kubista, *Spectrochim. Acta A Mol. Biomol. Spectrosc.*, 1995, **51**, L7-L21.
24. Z. Tak For Yu, H. Guan, M. Ki Cheung, W. M. McHugh, T. T. Cornell, T. P. Shanley, K. Kurabayashi and J. Fu, *Sci. Rep.*, 2015, **5**, 11339.
25. C. D. Chin, T. Laksanasopin, Y. K. Cheung, D. Steinmiller, V. Linder, H. Parsa, J. Wang, H. Moore, R. Rouse, G. Umviligihozo, E. Karita, L. Mwambarangwe, S. L. Braunstein, J. van de Wijgert, R. Sahabo, J. E. Justman, W. El-Sadr and S. K. Sia, *Nat. Med*, 2011, **17**, 1015-1019.
26. M. Grumann, A. Geipel, L. Riegger, R. Zengerle and J. Ducree, *Lab Chip*, 2005, **5**, 560-565.
27. R. P. Bagwe, C. Yang, L. R. Hilliard and W. Tan, *Langmuir*, 2004, **20**, 8336-8342.
28. R. P. Bagwe, L. R. Hilliard and W. H. Tan, *Langmuir*, 2006, **22**, 4357-4362.
29. A. Imhof, M. Megens, J. J. Engelberts, D. T. N. de Lang, R. Sprik and W. L. Vos, *J. Phys. Chem. B*, 1999, **103**, 1408-1415.
30. C. J. Moore, H. Monton, R. O'Kennedy, D. E. Williams, C. Nogues, C. Crean and V. Gubala, *J. Mater. Chem. B*, 2015, **3**, 2043-2055.
31. J.-H. Park, L. Gu, G. von Maltzahn, E. Ruoslahti, S. N. Bhatia and M. J. Sailor, *Nat. Mater*, 2009, **8**, 331-336.
32. V. Gubala, X. Le Guevel, R. Nooney, D. E. Williams and B. MacCraith, *Talanta*, 2010, **81**, 1833-1839.
33. S. J. Park, Y. J. Kim and S. J. Park, *Langmuir*, 2008, **24**, 12134-12137.
34. C. L. O'Connell, R. Nooney and C. McDonagh, *Biosens. Bioelectron.*, 2017, **91**, 190-198.
35. E. Mahon, D. R. Hristov and K. A. Dawson, *Chem. Commun.*, 2012, **48**, 7970-7972.
36. A. Salvati, A. S. Pitek, M. P. Monopoli, K. Prapainop, F. B. Bombelli, D. R. Hristov, P. M. Kelly, C. Aberg, E. Mahon and K. A. Dawson, *Nat Nanotechnol*, 2013, **8**, 137-143.
37. G. Blanco-Gomez, A. Glidle, L. M. Flendrig and J. M. Cooper, *Anal. Chem.*, 2009, **81**, 1365-1370.

1